

A Frequency Domain EM Algorithm to Detect Similar Dynamics in Time Series with Applications to Spike Sorting and Macro-Economics

Georg M. Goerg*

Carnegie Mellon University, Department of Statistics

November 12, 2022

Abstract

In this work I propose a frequency domain adaptation of the Expectation Maximization (EM) algorithm to separate a family of sequential observations in classes of similar dynamic structure, which can either mean non-stationary signals of similar shape, or stationary signals with similar auto-covariance function. It does this by viewing the magnitude of the discrete Fourier transform (DFT) of the signals (or power spectrum) as a probability density/mass function (pdf/pmf) on the unit circle: signals with similar dynamics have similar pdfs; distinct patterns have distinct pdfs. An advantage of this approach is that it does not rely on any parametric form of the dynamic structure, but can be used for non-parametric, robust and model-free classification. Applications to neural spike sorting (non-stationary) and pattern-recognition in socio-economic time series (stationary) demonstrate the usefulness and wide applicability of the proposed method.

*gmg@stat.cmu.edu

1 Introduction

Classification of similar signals is a widespread task in signal processing, where similar can either mean similar shape (for non-stationary signals), or similar dynamics (for stationary¹ signals). Non-stationary examples are recordings of brain activity (see Section 1.2) or speech signals; stationary signals can be found in many economic or physical time series. In both cases, researchers are interested in detecting similar dynamics:

Neuro-scientists study the signal shape sent by neurons in order to understand how fast neurons send information across the brain. As a recording can contain signals from many different neurons, it is necessary to cluster them into signals of similar shape (?), which presumably were sent by the same neuron.

In economics and public policy one is often interested in similar dynamics of the market/society to characterize, for example, how fast a country recovers from a recession, and how it compares to other countries in the region; or which countries have similar dynamics in their labor market.

Formally, let $\mathcal{X} = \{\mathbf{x}_{1,t}, \dots, \mathbf{x}_{N,t}\}$ be a family of sequential observations from a dynamical system \mathcal{S} , where $\mathbf{x}_{i,t} = (x_{i,1}, \dots, x_{i,T})$ is the individual time series of entity i . For example, \mathcal{S} can be a particular area in the brain or the economic rules in the labor market. Here we consider systems which can be naturally divided into K homogeneous sub-systems $\mathcal{S}_1, \dots, \mathcal{S}_K$, each one with its own characteristic dynamics. In the neurology context these sub-systems \mathcal{S}_k represent different neurons sending a signal; in economics \mathcal{S}_k could correspond to different dynamics in the market, e.g. countries that recover fast from a recession (\mathcal{S}_1) versus countries that need more time for their economy to catch up again to global economy (\mathcal{S}_2).

Many clustering and dimension reduction techniques such as principal component analysis (PCA) (?) focus on the mean and/or variance to make a reduction/classification in similar blocks of data. Interested in detecting similar dynamics over time in data, however, these two statistics are irrelevant for the correlation over time. ? even claim that time series clustering is entirely meaningless. However, ? show that time series clustering is not meaningless *per se*, but that care must

¹A sequence of random variables (RVs) $\{x_t\}_{t \in \mathbb{Z}}$ is stationary if i) $\mathbb{E}x_t = \mu < \infty$, ii) $\forall x_t := \mathbb{E}(x_t - \mu)^2 < \infty$ and iii) the auto-covariance function $\gamma(k) := \mathbb{E}(x_t - \mu)(x_{t-k} - \mu)$ is independent of t .

be taken in defining a proper similarity measure. In their work ? present optimal time-embeddings $x_t \rightarrow (x_{t-\tau_1}, x_{t-\tau_2}, \dots, x_{t-\tau_s})^\top \in \mathbb{R}^s$, $0 \leq \tau_1 < \tau_2 < \dots < \tau_s < T$ such that signals with different dynamics can be easily distinguished in the higher dimensional \mathbb{R}^s . This method works particularly well for long time series even with non-linear dynamics. However, if only few observations per series are available ($T \approx 100$ or even only 50), then time-embeddings are extremely sparse in \mathbb{R}^s and thus clustering becomes impractical.

For few observations it might be useful to first fit a model $\hat{\theta}_{j,t}$ to every series $\mathbf{x}_{j,t}$, and then cluster in the model space parametrized by $\{\hat{\theta}_1, \dots, \hat{\theta}_n\}$. ? present such a clustering methods for the broad class of auto-regressive integrated moving average (ARIMA) models. Although this works well for data with few observations, it suffers from a model selection bias: if we pick the wrong model for just some of the series, then the clustering cannot be accurate anymore. Furthermore, if the models are not nested in some sense, then it is hard to compare the parameters of $\mathbf{x}_{j,t}$ to the ones of $\mathbf{x}_{i,t}$.

Thus I propose a novel approach to clustering similar dynamics using frequency domain properties of the signals, which avoids the model selection bias and at the same time works even with few observations. In particular, treating the magnitude of the discrete Fourier transform (DFT) of signal $\mathbf{x}_{j,t}$ as a probability mass function (pmf) on the unit circle leads to a natural classification by an adaptation of the well-known Expectation Maximization (EM) algorithm (??). Section 3 describes a non-parametric version which avoids any kind of model selection bias. It can be easily adapted to a parametric framewor, e.g. to cluster time series in the model class of auto-regressive moving average processes.

1.1 Similar dynamics in socio-economic time series

In macro-economics and public policy researchers are often interested in comparing economies/societies with each other. For example, annual unemployment rates over the course of several decades can show changes in laws or adaptations of economic interdependencies within a country as well as with the rest of the world.

Here I will consider the annual per-capita income growth rate of the “lower 48” in the US from

1960 to 2008 compared to the overall US growth

$$g_{j,t} := r_{j,t} - r_{US,t}, \quad j \in \{\text{Alabama}, \dots, \text{Wyoming}\}, \quad (1)$$

where $r_{k,t}$ is the annual growth rate of region k (see Appendix A for details). Clustering states according to similar economic dynamics can help to decide where to provide economic support to overcome a recession faster. For example, if certain states do not show any important dynamics on a 7-8 year period - which is typically considered the “business cycle” (??) - then it might be more useful for to invest available money in those states that are heavily affect by these 7-8 year swings in economy.

This dataset has also been analyzed in ?, where the authors fit auto-regressive models of order 1 ($AR(1)$) to the non-adjusted growth rates $r_{j,t}$ for pre-selected 25 of the 48 states, and then cluster them based on the different fits. Although this procedure gives useful results, it is very unlikely that different dynamics for each of the 48 states only manifest themselves in a different $AR(1)$ coefficient. In particular, simple $AR(1)$ models cannot capture the business cycle dynamics which are clearly visible in the power spectra of the growth rates (even in the adjusted rates) - see Section 4.2, Fig. 3.

The non-parametric EM algorithm introduced in Section 3 does not face this model selection bias, but correctly captures different cyclic components in all of the 48 time series.

1.2 Neuron identification - “spike sorting”

The human brain can be seen as a big information-processing and -storing unit. For example, the information we get from watching our environment must be carried from the eye to the visual cortex - that area in the brain which can interpret this information. It is known that this visual cortex resides in the back of the brain. Thus neurons have to transmit information from the front to the back of the head, just for us to being able to make sense of what we see; set aside the neurons involved in executing our reaction to what we see. Every time a neuron transmits information it emits an electrochemical signal, which can be measured by an electrode put in the brain area of interest. Figure 1 (top) shows a recorded signal y_t with 73,500 observations.²

²For a detailed description see Appendix A.

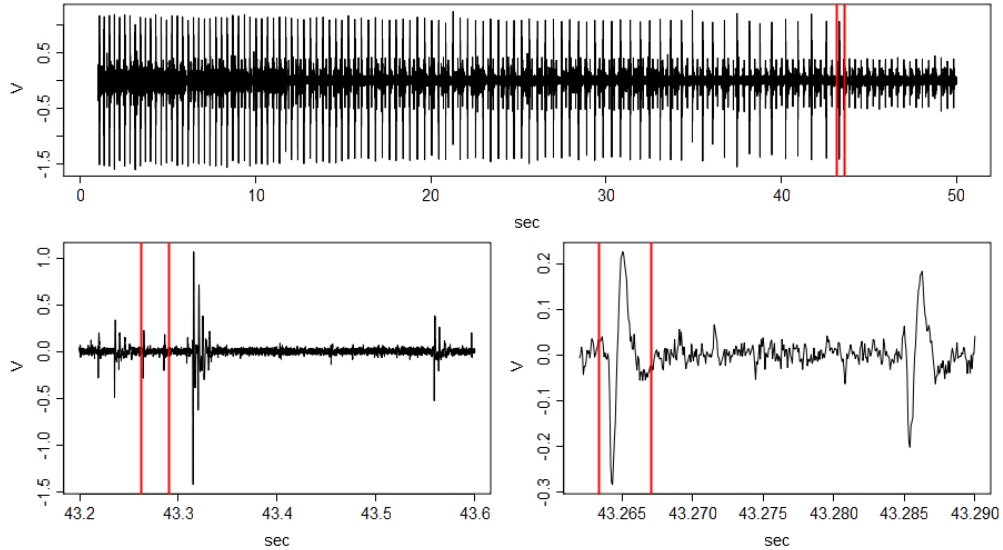


Figure 1: Brain signal recording: (top) entire 49 seconds; (bottom left) zoom into $[43.2, 43.6]$ - the transition between extremely large spikes (~ 43.3) and smaller spikes (~ 43.57); (bottom right) zoom into $[43.26, 43.29]$ where two spikes become visible

On a macro-level these measurements help to identify active areas of the brain which are involved in performing a particular task; e.g. for visual tasks the back of the brain shows up as an active area. Also the micro-level properties of neuron activity are important, for example ? analyze how fast neuron n_k can send information - this is characterized by the neuron's "firing rate". To do this non-trivial task, however, one implicitly makes an important assumption: it is known which neuron sent which signal. Figure 1 clearly shows that micro-electrodes cannot single out one neuron, but record a concatenation - and in the worst case a superposition - of an unknown number of neurons n_1, \dots, n_K transmitting information plus a lot of background noise.

Hence to successfully analyze the firing rates, it is necessary to

- i) distinguish actual spikes from background noise, and
- ii) identify and assign each signal to one particular neuron n_i , $i = 1, \dots, K$ where the number of neurons K is unknown: an electrode records as many neurons as there are in its local neighborhood.

Part i) constitutes one of the core problems in signal processing (??). Consequently there is an immense literature on signal/noise separation, especially in audio and speech processing (??). For sub-problem ii) the best we can do is classify the observed spikes into classes of similarly shaped

wave-forms. If these shapes actually correspond to one sole neuron n_i or still to a collection of neurons, depends on whether each neuron has a unique wave form or not. Only if there exists such a one-to-one relation, we can determine the firing rates of each single neuron. Biochemical and physiological findings suggest that each neuron has its own unique wave-form, which can only vary slightly based on the state of the neuron. Thus it should be possible to classify neuron activity according to the form of the signal - the “spike”. This classification task is commonly known as “spike sorting” (???)

A common and simple approach is performing PCA on the spikes, and then cluster the signals according to the PCA coefficients (?). Although generally there are far more spikes than observations in time ($N \gg T$), still the first 2-3 eigen-vectors of the low-rank correlation matrix capture most of the variation in the data. However, since PCA selects sources by the direction of maximum variance, it will classify low power firings from the same neuron as different neurons.

2 “Spike sorting” in the time domain

Put in a mathematical setting, let \mathcal{N} be the set of all neurons and assume that each neuron $n_i \in \mathcal{N}$ has a unique characteristic spike $S_i(t) \in \mathcal{C}[a, b]$, where $\mathcal{C}[a, b]$ is the set of all continuous functions on $[a, b]$. The spike is unique in the sense that $n_i = n_j$ if and only if $S_i(t) = S_j(t)$, or put in words if we see two different spikes, then we know that two different neurons were active and vice versa.

The micro-electrode only records a subset of neurons $n_i, i = 1, \dots, K$, where K is unknown. In Section 2.1 I use a slowness measure to distinguish between signal and noise, and in Section 4.1 I fit a Gaussian mixture model (GMM) to the slowness to detect different neurons, based on the assumption that a every different spike shape has its characteristic slowness.

2.1 Spike detection

Given the recorded signal y_t it is necessary to extract windows of size T containing a spike. These signals $s_{j,t}$ of length T represent the family of sequential observations $\mathcal{X} = \{s_{1,t}, \dots, s_{n,t}\} \in \mathbb{R}^{T \times N}$, where N is the number of detected spikes ($N \gg K, N \gg T$). The size of the window must match the length of a typical spike: the lower right panel of Fig. 1 suggests (vertical red lines) that a typical spike lasts for about 0.0035 seconds ≈ 55 time steps. Thus for the rest of this study I set

$T = 55$.

Since we do not know a-priori where a spike occurs we need a rule that tells us where to look for it. Whereas characterizing spikes visually is easy, designing a quantitative automated rule that can describe spikes is much more difficult. A common approach (?) is to set a threshold value tol and a spike is detected if the signal exceeds this threshold. However, the threshold rule will not only be very sensitive to outliers, but also bias the selected spikes in favor of spikes with large variance (power). This, however, misses the fact that sometimes neurons might fire with lower power than usual, and thus may not exceed such a threshold. Although missing these spikes would not affect the spike sorting algorithm, it will underestimate the firing rate of neuron n_i .

Here I characterize “non-spikes”, i.e. noise in a more suitable way, which actually detects spikes according to properties of the entire signal, not on single observations (such as the threshold rule). One way to characterize noise is that it is moving much faster than any spike - whatever such a spike may look like. ? introduced a measure of slowness for a signal x_t , defined as the variance of the differenced, unit-variance signal

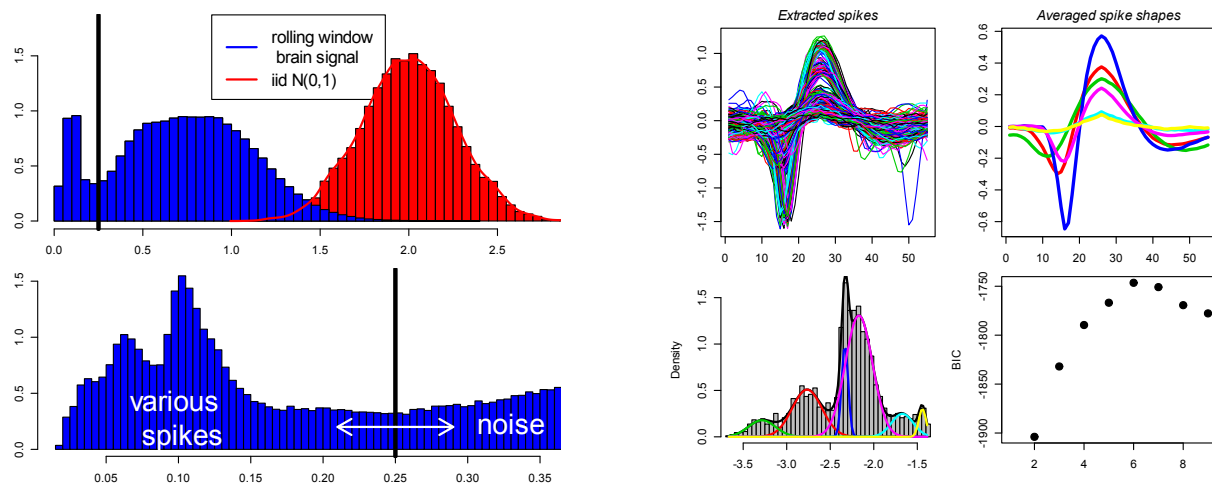
$$\Delta(x_t) = \mathbb{V}(x_t - x_{t-1}), \quad \mathbb{V}x_t = 1. \quad (2)$$

It follows that $\Delta(\text{const}) = 0$ and $\Delta(\varepsilon_t) = 2$ for ε_t being an independent identically distributed (iid) signal. Therefore, the higher $\Delta(x_t)$, the faster x_t .

Thus computing the slowness of the signal in a sliding window over y_t reveals noisy parts (fast) and - complementary - the spikes (slow). The red (right) histogram in Fig. 2a shows simulated $\Delta(\varepsilon_t)$, where $\varepsilon_t \stackrel{iid}{\sim} \mathcal{N}(0, 1)$ with $t = 1, \dots, T = 55$ for $N = 10,000$ replications. Clearly, the central limit theorem (CLT) comes into play and the simulated values are centered around their true slowness $\Delta(\varepsilon_t) = 2$.

However, there is no obvious reason to assume that the brain background noise in the neighborhood of the micro-electrode is necessarily iid. In fact, the empirical slowness (blue histogram) of the sliding windows is substantially lower than 2, showing that brain background noise is not iid.³ But even though we do not know how slow it is, we know - and can clearly see in Fig. 2a (bottom) - that noise moves much faster than any of the spikes - $\Delta(\text{brain noise}) \gg \Delta(\text{any spike})$. Hence, we

³Since $\Delta(\varepsilon_t) = \Delta(\text{const} \cdot \varepsilon_t)$ by definition ($\mathbb{V}x_t \equiv 1$ in (2)), the lower slowness for the brain signal is not just due to a lower variance white noise sequence, but indeed a manifestation of some dependence in the data.



(a) (top): (red) Simulation of $\Delta(\varepsilon_t)$ with 10,000 replications for iid $\{\varepsilon_t\}_{t=1}^{T=55}$; (blue) empirical slowness of the rolling window over the data y_t . (bottom): zoom into (0,0.4) with the boundary between spikes (< 0.25) and noise (> 0.25).

(b) (top) detected spikes; (below) their log slowness and a Gaussian mixture fit with 6 components (chosen according to BIC score)

Figure 2: How slowly do we think? - the slowness of brain recordings.

can learn the boundary value that distinguishes noise and spikes from the data. At this stage we are only concerned with separating spikes from noise, thus we can choose a conservative value for the boundary. If it turns out that this still includes too much noise, then a clustering algorithm will put these in a “noise” class. On the other hand, a too small boundary will miss spikes and thus bias the analysis of firing rates towards larger firing intervals. The lower panel of Figure 2a shows that choosing $tol = 0.25$ separates the data into lots of noise on the right, and spikes on the left.

This rolling window approach gives the so called on-set times (the moment a neuron fires and the spike lasts for $T = 55$ units of time), which are then used to extract possible spikes $s_{j,t}$ from y_t . An additional alignment step takes place to avoid slight misplacements of the onset times; following the spike sorting literature, this was done by identifying the maximum of each spike and adjust the window such that all signals have their maximum at the same position.

Figure 2a shows $n = 1,747$ extracted signals of length $T = 55$ obtained by applying the slowness measures on a sliding window using $tol = 0.25$. The rolling window spike detection could not exclude noise completely, so in the upper left panel of Fig. 2b one can distinguish 2-3 spikes and some noise. However, this does not hurt the classification since the clustering algorithm can put remaining noise

in the class “noise”. Even though the low-variance signals seem to be noise, they could also be just low-power spikes. Since the slowness measure is invariant to scaling, it does not falsely ignore low power signals.

Before applying a standard classification algorithm on the extracted signals in Section 4, I first describe the main contribution of this work.

3 Non-parametric, frequency domain EM algorithm

As already mentioned in the Introduction dynamic clustering methods are not feasible if a) only few observations are available (ruling out time-embedding) and b) assuming specific models is not desired as it leads to an unnecessary model selection bias (as for economic time series).

Here I propose a novel approach to clustering dynamic structures in time series, by identifying each time series with the distribution it induces on the unit circle - and thus on the interval $[-\pi, \pi]$ - by its Fourier transform.

Definition 3.1 (Spectral Density). *The spectral density of a stationary, zero-mean time series x_t with auto-covariance function $\gamma(\ell) = \mathbb{E}x_t x_{t-\ell}$ is defined as*

$$f_x(\lambda) := \frac{1}{2\pi} \sum_{\ell=-\infty}^{\infty} \gamma(\ell) e^{i\lambda\ell}, \quad \lambda \in [-\pi, \pi], \quad (3)$$

where the limit is understood point-wise if $\{\gamma(\ell)\}_{\ell=-\infty}^{\infty}$ is absolutely summable, and in the mean-square sense if $\{\gamma(\ell)\}_{\ell=-\infty}^{\infty}$ is square summable.

For real valued processes $\gamma(\ell) = \gamma(-\ell)$, thus $f_x(\lambda) \geq 0$ for all λ . Furthermore,

$$\int_{-\pi}^{\pi} f_x(\lambda) d\lambda = \sigma_x^2, \quad (4)$$

since $\int_{-\pi}^{\pi} e^{i\lambda\ell} d\lambda = 0$ if $\ell \neq 0$ and $\gamma(0) = \sigma_x^2$. Equivalence (4) is also known as the spectral decomposition of the variance of a time series. Hence, the spectral density is a non-negative function on the interval $[-\pi, \pi]$ and peaks at λ_0 indicate that this frequency is important for the overall variance of the process, since peaks in $f_x(\lambda)$ contribute a lot to the integral (4).

An estimate of the spectral density is the power spectrum or *periodogram*.

Definition 3.2 (Periodogram). *The periodogram (or power spectrum) of x_t is defined as*

$$I_{T,x}(\omega_j) := |X(\omega_j)|^2 = \left| \frac{1}{\sqrt{T}} \sum_{k=0}^{T-1} x_k e^{-2\pi i \omega_j k} \right|^2, \quad \omega_j = j/T, \quad j = 0, 1, \dots, T-1 \quad (5)$$

where ω_j are the Fourier frequencies (scaled by 2π for easier interpretation).

For large T a frequent model for $I_{T,x}(\omega_j)$ is (see ?)

$$I_{T,x}(\omega_j) = f_x(\omega_j)\eta, \quad j = 0, \dots, T-1, \quad (6)$$

where η is a standard (rate = 1) exponential RV. Thus at each frequency ω_j , the periodogram is modeled as an exponential RV with rate parameter equal to the true spectral density $f_x(\omega_j)$. Therefore $\mathbb{E}I_{T,x}(\omega_j) = f_x(\omega_j)$ and $\text{Var}I_{T,x}(\omega_j) = f_x(\omega_j)^2$; thus $I_{T,x}(\omega_j)$ is asymptotically unbiased, but not consistent. This is especially harmful for large values of the true spectral density, as they exactly correspond to those frequencies which are particularly important for the overall variation. Common approaches to make the variance converge to 0 for $T \rightarrow \infty$ is a windowing approach where the periodogram at ω_j is averaged over an increasing (with T) number of neighboring frequencies (?). Again this works well for series with many observations, but for small samples such as the neuron spikes or many economic time series averaging over neighboring frequencies is not a practical option.

However, for M independent time series $\{x_{m,t}\}_{m=1}^M$ of the same type (all from sub-system \mathcal{S}_k) an estimate of the true $f_{\mathcal{S}_k}(\lambda)$ can be obtained by averaging over the M periodograms at each frequency

$$\widehat{f}_{\mathcal{S}_k}(\lambda) |_{\lambda=\omega_j} = \frac{1}{M} \sum_{m=1}^M I_{T,x_{m,t}}(\omega_j), \quad j = 0, \dots, T-1. \quad (7)$$

Since by assumption all $x_{m,t} \in \mathcal{S}_k$ have the same dynamic structure, $\widehat{f}_{\mathcal{S}_k}(\lambda)$ is also a good estimate of $f_{x_{m,t}}(\lambda)$ for all $m = 1, \dots, M$.

If the sub-series $x_{m,t}$ are far enough apart in a signal y_t , then periodograms $I_{T,x_{m,t}}(\omega_j)$ can be considered as independent samples of the same underlying true spectral density $f_{\mathcal{S}_k}(\lambda)$. Thus (7)

is still unbiased, and has considerably lower variance

$$\mathbb{E}\widehat{f}_{\mathcal{S}_k}(\omega_j) = f_{\mathcal{S}_k}(\omega_j), \quad \mathbb{V}\widehat{f}_{\mathcal{S}_k}(\omega_j) = \frac{f_{\mathcal{S}_k}(\omega_j)}{M}. \quad (8)$$

Recall that each neuron n_k , $k = 1, \dots, K$ has its own characteristic shape (represented by \mathcal{S}_k) which reflects in a characteristic Fourier transform, and thus spectral density $f_{\mathcal{S}_k}(\lambda)$.

Equation (7) looks very similar to the M step of an EM algorithm (?). In fact, the periodogram can be interpreted as probability mass functions (pmf) on ω_j , $j = 0, \dots, T - 1$, thus based on (7) I introduce a non-parametric EM algorithm in the frequency domain, to obtain consistent estimates of the spectral density, with the by result of a very general, non-parametric classification algorithm for any kind of data with a spectral representation, which is not only restricted to sequential data, but can also be use for clustering images (2D Fourier transform) as well as classification of a family of positive semi-definite random matrices $\{A_i\}_{i=1}^N$ considering their normalized eigenvalue spectrum $\{\lambda_j\}_{j=1}^{\dim(A_i)}$ as a discrete distribution on $j = 1, \dots, \dim(A_i)$.

Consider a set of observations $\Lambda = \{\lambda_1, \dots, \lambda_N\}$, $\lambda_i = (\lambda_{i,0}, \dots, \lambda_{i,T-1})$, from a mixture distribution

$$p(\lambda \mid \theta_1, \dots, \theta_K; \pi_1, \dots, \pi_K) = \sum_{k=1}^K \pi_k p(\lambda \mid \theta_k), \quad (9)$$

where θ_j can either represent a parameter vector of just indicate that there are K different pdfs $p(\lambda \mid \cdot)$. Since $f_x(\lambda)$ is a well-defined continuous pdf for unit-variance x_t , $p(\lambda \mid \theta_k)$ can be identified with $f_{\mathcal{S}_k}(\lambda)$. As we do not observe the Fourier frequencies $\lambda_i = (\lambda_{i,0}, \dots, \lambda_{i,T-1})$ we cannot use MLE directly. However, eq. (20) in the Appendix B shows how to compute the value of the log-likelihood of λ_i as a linear combination of Kullback-Leibler (KL) divergences and the entropy of λ_i . Thus it is possible to employ a non-parametric frequency domain EM algorithm by estimating the “true” densities $f_{\mathcal{S}_k}(\lambda)$ non-parametrically by averaging over all periodograms of signals of sub-system \mathcal{S}_k :

0. Initialization: set $\tau = 0$ and randomly assigning $\mathbf{x}_{i,t}$ to one of the K sub-systems; define

$$\gamma_{ik}^{(\tau)} := 1 \text{ if } \mathbf{x}_{i,t} \in \mathcal{S}_k; 0 \text{ otherwise.}$$

1. Estimate $f_{S_k^*}(\lambda)$ by a weighted average of the periodograms of $\mathbf{x}_{i,t}$:

$$\widehat{f}_{S_k^*}^{(\tau)}(\omega_j) = \sum_{i=1}^N w_{ik^*}^{(\tau)} I_{\mathbf{x}_{i,t}}(\omega_j), \quad w_{ik^*}^{(\tau)} = \frac{\gamma_{ik^*}^{(\tau)}}{\sum_j \gamma_{jk^*}^{(\tau)}} \text{ for each } k^* = 1, \dots, K. \quad (10)$$

This gives K spectral densities $\mathcal{F}^{(\tau)} = \{\widehat{f}_{S_1}^{(\tau)}, \dots, \widehat{f}_{S_K}^{(\tau)}\}$ at iteration τ . Note that for each k^* it holds $\mathbb{E} \widehat{f}_{S_k^*}^{(\tau)}(\omega_j) = f_{S_k^*}(\omega_j)$ and $\mathbb{V} \widehat{f}_{S_k^*}^{(\tau)}(\omega_j) \approx \frac{f_{S_k^*}(\omega_j)}{\sum_j \gamma_{jk^*}^{(\tau)}} \ll f_{S_k^*}(\omega_j)$.

2. Compute KL divergence between each $I_{\mathbf{x}_{i,t}}(\omega_j)$ and all $\widehat{f}_{S_k^*}^{(\tau)} \in \mathcal{F}^{(\tau)}$:

$$\mathcal{D}_{KL} \left(I_{\mathbf{x}_{i,t}} \parallel \widehat{f}_k^{(\tau)} \right) = \sum_{k=0}^{T-1} I_{\mathbf{x}_{i,t}}(\omega_j) \log \frac{I_{\mathbf{x}_{i,t}}(\omega_j)}{\widehat{f}_k^{(\tau)}(\omega_j)}, \quad \forall j, \forall k^* \quad (11)$$

3. update probability

$$\gamma_{ik}^{(\tau+1)} = \mathbb{P}(\mathbf{x}_{i,t} \in S_k) = \mathbb{P}(\mathbf{x}_{i,t} \mid \theta_k = \widehat{f}_{S_k}^{(\tau)}), \quad \forall i, \forall k \quad (12)$$

using (21) and (11). Set $\tau = \tau + 1$.

4. repeat steps 1 - 3 until convergence of the overall likelihood $\log p(\lambda \mid \theta_1, \dots, \theta_K; \pi_1, \dots, \pi_K)$.

Since for unit-variance input x_t the spectral density/periodogram are well-defined continuous/discrete probability distributions, this EM algorithm can be applied to both stationary as well as non-stationary signals: in the first case, the spectral density $f_x(\lambda)$ exists as a non-negative, square integrable function and a large part of the time series and econometrics literature is devoted to the spectral analysis of stationary time series (??); in the second case, the periodogram (5), viewed as a purely data-driven method, still provides a valid discrete pmf on $\{\omega_j\}_{j=0}^{T-1}$.

Since frequency domain analysis plays a very prominent and successful role in statistics, time series analysis, and signal processing, the frequency domain EM algorithm to detect similar dynamics or shape can be easily implemented and applied to a great variety of problems.

It must be noted though that it comes with all the pros and cons of the basic EM algorithm (never decreasing likelihood, but possibly local optima). For a detailed account of convergence results, and many other properties see ? or ?.

Table 1: EM estimates of a 6 component GMM for $\log \Delta(s_{j,t})$

	Comp 1	Comp 2	Comp 3	Comp 4	Comp 5	Comp 6
π_k	0.069	0.218	0.093	0.511	0.078	0.031
μ	-3.285	-2.766	-2.331	-2.171	-1.671	-1.442
σ^2	0.155	0.171	0.037	0.156	0.125	0.042

4 Results

In this section I demonstrate the usefulness and wide applicability of the presented methods on neuron spike train data (non-stationary) and the income growth data (stationary).

4.1 Spike sorting

For the neuron classification we can either try to fit a mixture model directly on the T - dimensional data, or compute “features” for each spike that summarize its shape. A good feature selection will reduce the dimensionality of the data, and thus greatly accelerate computations.

Here I will cluster both in the time and frequency domain: for the first I fit a Gaussian mixture model (GMM) on the logarithm of the slowness of each spike, $\log \Delta(s_{j,t})$; for the second I use the frequency domain EM algorithm (see Section 3) on the power spectra induced by each series $s_{j,t}$.

4.1.1 Gaussian mixture model on slowness

The histogram in Fig. 2b of $\{\log \Delta(s_{j,t})\}_{j=1}^{1,747}$ shows 5-6 peaks, which presumably correspond to 5-6 differently shaped spikes. Thus I fit GMMs to $\log \Delta(s_{j,t})$ and assign each spike $s_{j,t}$ to the cluster with highest a posteriori probability. Table 1 shows parameter estimates of the 6 component model, which was chosen according to the highest BIC score (Fig. 2b) from all GMMs up to order 10.⁴

The corresponding spikes are shown in the upper right panel of Fig. 2b. As $tol = 0.25$ was too conservative, two shapes still represent noise, and GMM identifies $K = 4$ different neurons.

4.1.2 Clustering in the frequency domain

After time-domain techniques, I use the frequency domain EM algorithm described in Section 3 to sort the spikes. An additional advantage of working in the frequency domain compared to the

⁴To avoid local maxima, I ran the EM algorithm (package `mixtools` in R) 100 times for each number of components and chose the largest local optimum solution for each number of components.

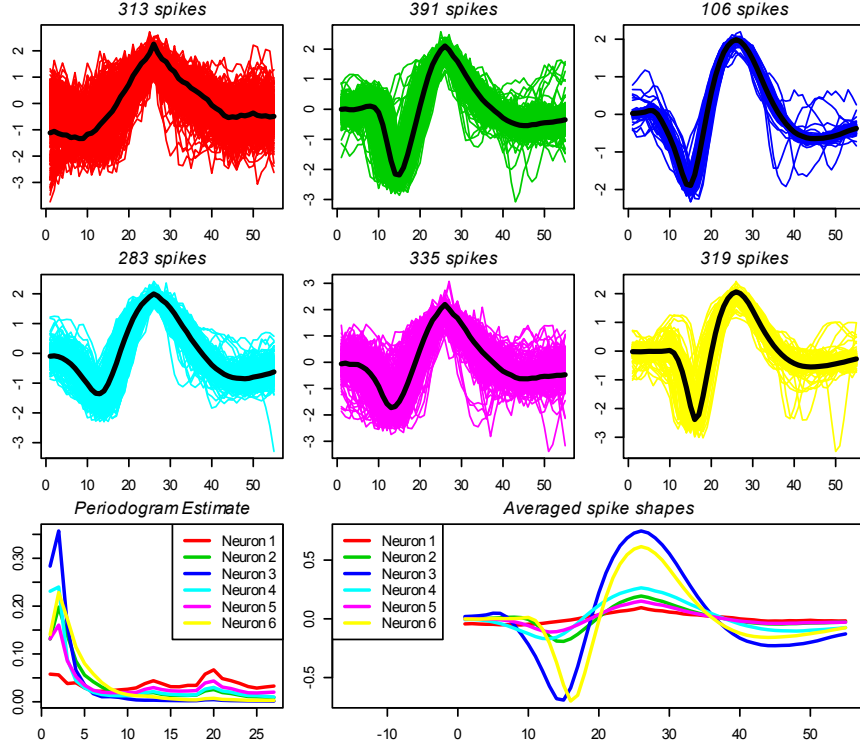


Figure 3: EM on periodograms of differenced spike signals $s_{j,t} - s_{j,t-1}$

time-domain: misalignment of the spikes does not affect the clustering.

Since I use the non-parametric version of the EM, the BIC criterion is not a suitable indicator for model complexity, as already 2 components are too complex in the BIC sense (treating every frequency estimate as one parameter).⁵ For easier comparison to the GMM model, I also use 6 classes $\{f_{S_1}, \dots, f_{S_6}\}$. The frequency approach puts all noise in one class (one flat spectrum in the lower left part of Fig. 3), and detects $K = 5$ different shapes.

4.2 States with similar income dynamics in the US

Applying the same algorithm to the (more or less) stationary income growth rate data yields 3 dominant dynamics in the income growth structure in the US, which are shown in Fig. 4. The x-axis of the periodograms (3 upper left panels) is the Fourier frequency ω_j . Their interpretation is as follows: peaks in the spectral density/periodogram at frequency ω_j mean that periods of length $1/\omega_j$ are important for the variation in the data.

⁵Future work can be done in an adaptation of the EM algorithm to parametric models, for which the BIC criterion indeed can be used.

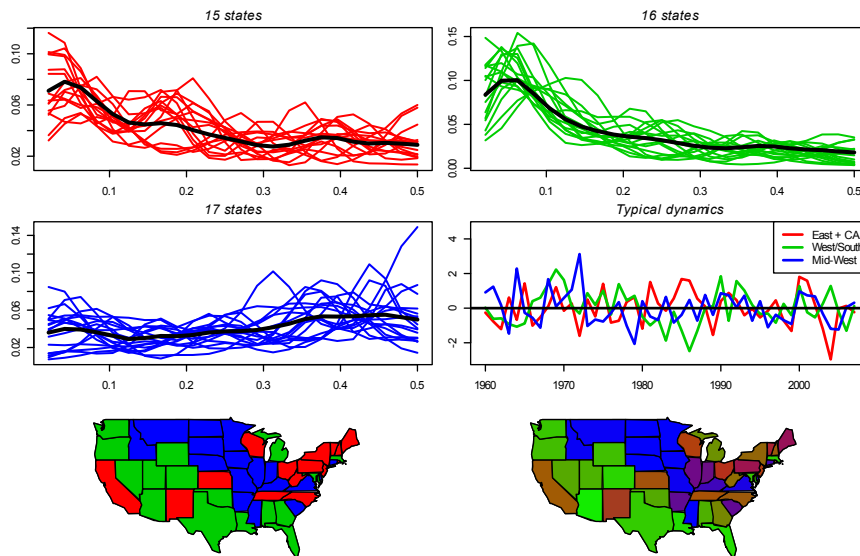


Figure 4: Non-parametric, frequency domain EM detects 3 dominant dynamics of per-capita income growth (3 upper-left panels); (center-right) representative average income growth of the 3 classes; (bottom) color coded map: (left) hard assignment, (right) soft assignment (RGB = $(\hat{\gamma}_{j1}, \hat{\gamma}_{j2}, \hat{\gamma}_{j3})$).

For example, the red series (East coast & CA) exhibits important slow frequencies (long cycles); in particular, two important cycles stand out: $\omega \approx 0.04$ and $\omega \approx 0.16$. These two correspond to a cycle length of 25 years and 6-7 years – which represent a generation cycle and the business cycle (?). The blue series on the other hand, does not show clear peaks, but has a flat spectrum: it is neither affected by short nor by long range dynamics. The green series has a generation cycle, but no visible business cycle. Note that $AR(1)$ models (?) may be appropriate for the green and blue dynamics ($AR(1)$ coefficient close to 1 and 0, respectively), but cannot capture two cycles as shown in the red series.

Thus the non-parametric EM algorithm on the periodograms separates US income dynamics over the last 50 years in 3 major types:⁶

\approx **East & CA (red)**: economy is highly persistent, changes are slow; business cycle of $\approx 6-7$ years is also important;

\approx **West/South (green)**: also highly persistent, but not affected by global business cycle;

\approx **Mid-West (blue)**: no persistence, only higher frequencies are slightly more important; decou-

⁶Any resemblance of the RGB color system to politics is purely coincidental.

pled from global business cycle.

One possible explanation why the blue states have a flat spectrum, is that these are majorly agricultural states, and since people have to eat no matter how the global economy is doing, the blue states income is not affected too much by recession or other market fluctuations. On the contrary, states whose economy - and thus income - relies heavily on industry, production, or technology are more affected by global economy swings, which typically happen every 7-8 years.

Hence, the classification in Fig. 4 can provide a basis for more effective policies to boost local economies facing a recession: it might be more effective to allocate main parts of public investments to states that are actually affected by the business cycle, and not put it in states which are decoupled from global economy.

5 Discussion and Outlook

In this work I introduce a novel technique to detect and classify similar dynamics in signals, where similar dynamics can either mean similar shape for non-stationary signals, or similar auto-correlation for stationary signals. It is an adaptation of the EM algorithm to the power spectra of the signals and thus benefits from the extensive literature in both areas of signal processing. Applications to neural spike sorting and pattern recognition in macro-economic time series demonstrate the usefulness of the presented method.

I also used the recently introduced slowness feature for the classification of neuron spikes. The slowness of signals can i) separate signals from noise, and ii) also distinguish differently shaped signals. Compared to multivariate methods in the literature it is very fast and easily computable, and much more robust to outliers than for example the standard approach of exceeding a threshold.

A Data

Spikes The data y_t are recordings of an electro-chemical signal in the cerebral slice of a rat.⁷ A band pass filter for frequencies between 300 Hz and 5 kHz has been applied to y_t , which was sampled at a rate of 15 Khz for 1 minute.

⁷This PKdata set can be obtained from www.biomedicale.univ-paris5.fr/phycerv/C_Pouzat/Data.html.

Income The dataset can be obtained from www.bea.gov/regional/spi. It contains the average per-capita income of the “lower 48” states and the entire US: $I_{j,t}$, $j = 1, \dots, 49$. As usual, all $I_{j,t}$ grow exponentially with time, so one typically analyzes the growth rate $r_{j,t} := \log I_{j,t} - \log I_{j,t-1}$ - also known as log-returns - which is (more or less) stationary. Since we are interested in the individual dynamics of a state compared to the US, I analyze the difference between the state growth rate and the US growth rate, as this is a finer indicator of the state’s dynamics (data-wise it removes the overall seasonal trend of the US baseline). Additionally, removing the overall growth is more apt for the money allocation decision scenario within the US.

B KL divergence and Maximum Likelihood

Let $p_k := \mathbb{P}(X = a_k)$ define a probability distribution for the RV X taking values in the finite alphabet $\mathcal{A} := \{a_1, \dots, a_K\}$. The Kullback-Leibler (KL) divergence between two discrete probability distributions $p = \{p_1, \dots, p_K\}$ and $q = \{q_1, \dots, q_K\}$

$$\mathcal{D}_{KL}(p \parallel q) := \sum_{i=1}^K p_i \log_2 \frac{p_i}{q_i} = \mathbb{E}_p \log_2 \frac{p_i}{q_i} \quad (13)$$

measures how far p and q are apart; in particular, if $p = q$ then $\mathcal{D}_{KL}(p \parallel q) = 0$.

Let $\tilde{p}(x)$ be the empirical distribution function (edf) of a sample $\mathbf{x} = (x_1, \dots, x_N)$

$$\tilde{p}(\mathbf{x}) := \sum_{n=1}^N \delta(x - x_n), \quad (14)$$

where $\delta(y)$ is the Dirac delta function, and let $p(\mathbf{x} \mid \theta)$ be a model (distribution) for the RV X . The maximum likelihood estimator (MLE) is a common method to estimate θ from \mathbf{x} . It is defined as that θ which maximizes the log-likelihood of the data

$$\ell(\theta \mid \mathbf{x}) := \sum_{n=1}^N \log p(x_n \mid \theta). \quad (15)$$

In terms of the KL divergence it is intuitive to select that θ which minimizes the distance between

the empirical distribution of the data $\tilde{p}(\mathbf{x})$ and the model $p(\mathbf{x} | \theta)$. In fact, they are equivalent since

$$\mathcal{D}_{KL}(\tilde{p}(\mathbf{x}) || p(\mathbf{x} | \theta)) = \int \tilde{p}(\mathbf{x}) \log \frac{\tilde{p}(\mathbf{x})}{p(\mathbf{x} | \theta)} d\mathbf{x} = -H(\tilde{p}(\mathbf{x})) - \int \tilde{p}(\mathbf{x}) \log p(\mathbf{x} | \theta) d\mathbf{x}, \quad (16)$$

where $H(\tilde{p}(\mathbf{x})) = \int \tilde{p}(\mathbf{x}) \log \tilde{p}(\mathbf{x}) d\mathbf{x}$ is the entropy of $\tilde{p}(\mathbf{x})$, which is independent of θ . Thus

$$\arg \min_{\theta} \mathcal{D}_{KL}(\tilde{p}(\mathbf{x}) || p(\mathbf{x} | \theta)) = \arg \max_{\theta} \mathbb{E}_{\tilde{p}} \log p(\mathbf{x} | \theta). \quad (17)$$

Plugging (14) in the right hand side of (17) shows the equivalence of KL divergence minimization and log-likelihood maximization as

$$\mathbb{E}_{\tilde{p}} \log p(\mathbf{x} | \theta) = \frac{1}{N} \int \sum_{n=1}^N N \delta(x - x_n) \log p(x | \theta) dx = \frac{1}{N} \sum_{n=1}^N \log p(x_n | \theta) \quad (18)$$

$$= \frac{1}{N} \ell(\theta | \mathbf{x}). \quad (19)$$

Thus the log-likelihood of \mathbf{x} can be computed by

$$\ell(\theta | \mathbf{x}) = -N \cdot [\mathcal{D}_{KL}(\tilde{p}(\mathbf{x}) || p(\mathbf{x} | \theta)) + H(\tilde{p}(\mathbf{x}))], \quad (20)$$

and consequently

$$\mathbb{P}(\mathbf{x} | \theta) = e^{\ell(\theta | \mathbf{x})}. \quad (21)$$

Equations (20) and (21) play a key role in the non-parametric EM algorithm defined on the power spectra, as they allow to compute $\ell(\theta | \mathbf{x})$ even though \mathbf{x} has not been observed directly, but just its edf $\tilde{p}(\mathbf{x})$ and a model $p(\mathbf{x} | \theta)$. In this framework, the data \mathbf{x} are the unobserved Fourier frequencies $\omega_0, \dots, \omega_{T-1}$, the edf $\tilde{p}(\mathbf{x})$ translates to the periodogram $I_T(\omega_k)$, and the “true” model $p(\mathbf{x} | \theta)$ is the EM estimate $\hat{f}_{\mathcal{S}_k}(\lambda) |_{\lambda=\omega_j}$ of the spectral density of sub-system \mathcal{S}_k - see (10).